Available online at www.sciencedirect.com

ScienceDirect

IFAC PapersOnLine 52-15 (2019) 247–252

# Generalized Lyapunov Demodulator for Amplitude and Phase Estimation by the Internal Model Principle

**Michael R. P. Ragazzon** * **Saverio Messineo** **
**Jan Tommy Gravdahl** * **David M. Harcombe** ***
**Michael G. Ruppert** ***

* *Department of Engineering Cybernetics, Norwegian University of Science and Technology (NTNU), Norway (e-mail: michael.remo.ragazzon@ntnu.no, jan.tommy.gravdahl@ntnu.no)*
** *Department of ICT and Natural Sciences, NTNU (e-mail: messineo.saverio@ntnu.no)*
*** *School of Electrical Engineering and Computing, University of Newcastle, Australia, (e-mail: michael.ruppert@newcastle.edu.au, david.harcombe@uon.edu.au)*

**Abstract:** Effective demodulation of amplitude and phase is a requirement in a wide array of applications. Recent efforts have increased the demodulation performance, in particular, the Lyapunov demodulator allows bandwidths up to the carrier frequency of the signal. However, being inherently restricted to a single order filtering of the input signal, signal components outside its passband are not sufficiently attenuated for all applications, such as in multifrequency atomic force microscopy. In this article, the structure of the Lyapunov demodulator is transformed to an equivalent form, taking advantage of the internal model representation of the sinusoid to be tracked. A generalization of this formulation allows the application of standard filtering techniques in order to shape the characteristics of the demodulator, while retaining the perfect tracking condition provided by the internal model. Guidelines for the filter design are provided in order to achieve the desired characteristics, such as filtering order, tracking bandwidth, and transient performance. The resulting generalized Lyapunov demodulator structure is highly flexible, allows for direct employment of any standard filter type, is computationally simple, and easy to implement requiring only a bandpass filter, a single integrator, and two nonlinear transformations. Numerical results demonstrate the effectiveness of the approach, and provide a comparison of the various filters considered.



*Keywords:* demodulators, estimation, internal model principle, atomic force microscopy, bandpass filters, closed-loop transfer functions

## 1. INTRODUCTION

The Lyapunov amplitude and phase demodulator explored in Ragazzon et al. (2018b) shows promising features for implementation in many practical applications, such as in atomic force microscopy (AFM). In dynamic mode AFM applications, the demodulator is placed directly in the vertical axis feedback loop, thereby imposing a limitation on the achievable bandwidth and scanning speed of the microscope (Abramovitch et al., 2007; Garcia and Perez, 2002). The Lyapunov demodulator compares favorably in several aspects to state-of-the-art techniques, demonstrating one of the highest tracking performances with bandwidths reaching the carrier frequency of the signal, combined with simplicity of implementation (Ruppert et al., 2017).

However, with the recent emergence of multifrequency AFM enabling the investigation of material properties (Garcia and Herruzo, 2012; Cartagena-Rivera et al., 2015; Dufrêne et al., 2017; Herruzo et al., 2014; Ragazzon et al., 2018a), the ability for multifrequency demodulation has become a key requirement. Here, the demodulator must be able to separate several frequency components simultaneously from a single signal (Harcombe et al., 2018; Ruppert et al., 2016).

The widely used lock-in amplifier when combined with a high order filter, achieves (i) high attenuation of frequency components away from the carrier frequency (off-mode rejection), and (ii) effective noise filtering at higher frequencies (Ruppert et al., 2017). The former being an essential performance metric in multifrequency demodulation. However, its tracking bandwidth is severely limited compared to the Lyapunov demodulator. On the other hand, the Lyapunov demodulator acts as a single-order filter, thus comparing unfavorably in terms of off-mode rejection. Combining their strengths would produce the ideal demodulator.

In Ruppert et al. (2018), a linear time-invariant (LTI) model of the standard Lyapunov demodulator is derived, which allows for the direct design of closed-loop demod-


10.1016/j.ifacol.2019.11.682

ulators with higher order Butterworth and Chebyshev filter characteristics. However, limitations in the degrees of freedom of the controller parameterization requires pole placement optimization to address non-minimum phase zeros in the overall response.

In this article, the need for controller parameterization is circumvented; rather, the desired closed-loop filter shape can be designed and implemented directly by any standard bandpass filter without modifications. By structuring the system around an internal model of the input sinusoid, the conditions under which perfect tracking is guaranteed is found. Furthermore, the perfect tracking conditions can be relaxed in order to improve the demodulator response over the entire tracking bandwidth. The result is a flexible demodulator achieving both high filter order and high tracking bandwidth simultaneously.

The article proceeds as follows. First, the measured sinusoid is treated as a reference signal to be tracked. Then, the standard Lyapunov demodulator is equivalently recast to an LTI system formulation, taking advantage of the internal model principle and thereby enabling perfect tracking of the sinusoid (Goodwin et al., 2000; Francis and Wonham, 1976; Messineo and Serrani, 2009). The reformulated system is generalized by employing an internal filter. Then, it is demonstrated that the feedback loop of the generalized demodulator can be designed directly as a bandpass filter, thereby enabling standard filtering techniques while still satisfying the perfect tracking condition. Then, filter design examples present higher order versions of the standard Lyapunov demodulator, in addition to common bandpass filters for use in the generalized Lyapunov demodulator. Finally, numerical examples demonstrate the increased offmode rejection achieved compared to the standard Lyapunov demodulator.

## 2. LYAPUNOV DEMODULATOR

Given the signal

$$r(t) = a\sin(\omega_c t + \varphi) \tag{1}$$

with unknown amplitude $a$ and phase $\varphi$, and known carrier frequency $\omega_c$, the demodulation problem considered is the online estimation of $a, \varphi$ purely based on the measurement of $r$.

The standard Lyapunov demodulator for estimation of amplitude and phase (Ragazzon et al., 2018b) can be written as

$$\begin{aligned} \dot{\boldsymbol{x}} &= \gamma \boldsymbol{c}\varepsilon, \\ y &= \boldsymbol{c}^T\boldsymbol{x}, \end{aligned} \tag{2}$$

where $\varepsilon = r - y$, the constant parameter $\gamma > 0$ determines the demodulation bandwidth, the state vector $\boldsymbol{x} = [x_1,\, x_2]^T$ and the signal vector $\boldsymbol{c}$ is given by

$$\boldsymbol{c} = [\cos(\omega_c t),\, \sin(\omega_c t)]^T. \tag{3}$$

Furthermore, the estimated amplitude $\hat{a}$ and phase $\hat{\varphi}$ can then be recovered from

$$\hat{a} = \sqrt{x_1^2 + x_2^2}, \quad \hat{\varphi} = \operatorname{atan2}(x_1, x_2), \tag{4}$$

where $\operatorname{atan2}(\cdot)$ is the four-quadrant inverse tangent function. As will be shown, it turns out that the structure of the standard Lyapunov demodulator is especially suitable for application of the internal model principle.

## 3. GENERALIZED LYAPUNOV DEMODULATOR

In the following, the structure of the standard Lyapunov demodulator is recast and generalized to allow for application of arbitrary filtering techniques.

### *3.1 Internal Model Representation*

The problem of estimating amplitude and phase of $r(t)$ can equivalently be recast as follows. To begin with, the sinusoidal signal $r(t)$ can be seen as generated by the output of the following system

$$\begin{aligned} \dot{\boldsymbol{w}} &= \mathbf{S}\boldsymbol{w} \\ \boldsymbol{w}(0) &= \boldsymbol{w}_0 \\ r(t) &= \boldsymbol{\Gamma}^T\boldsymbol{w} \end{aligned} \tag{5}$$

with $\boldsymbol{\Gamma} = [1, 0]^T$ and

$$\mathbf{S} = \begin{bmatrix} 0 & \omega_c \\ -\omega_c & 0 \end{bmatrix} \tag{6}$$

which implies that

$$e^{\mathbf{S}t} = \begin{bmatrix} \cos\omega_c t & \sin\omega_c t \\ -\sin\omega_c t & \cos\omega_c t \end{bmatrix}. \tag{7}$$

By the change of coordinates $\boldsymbol{v} = e^{\mathbf{S}t}\boldsymbol{x}$ applied to (2), the following system is retrieved,

$$\begin{aligned} \dot{\boldsymbol{v}} &= \mathbf{S}\boldsymbol{v} + \gamma\boldsymbol{\Gamma}\varepsilon \\ y &= \boldsymbol{\Gamma}^T\boldsymbol{v}. \end{aligned} \tag{8}$$

System (8) is said to incorporate an *internal model* of the sinusoidal signal $r(t)$ (Francis and Wonham, 1976).

### *3.2 Generalized Lyapunov Demodulator*

As the standard Lyapunov demodulator is a relative order 1 filter, there is a desire to increase the filtering order which can only be achieved through additional design degrees-of-freedom. A natural extension of the system (8) replaces the pure gain $\gamma$ by a filter

$$\begin{aligned} \dot{\boldsymbol{\eta}} &= \mathbf{A}\boldsymbol{\eta} + \mathbf{B}\varepsilon \\ u &= \mathbf{C}\boldsymbol{\eta} \end{aligned} \tag{9}$$

where $\mathbf{A} \in \mathbb{R}^{m\times m}$ is Hurwitz and $m$ being a design parameter. Then, from (8),(9), the overall extended version of the Lyapunov demodulator can be written as follows

$$\begin{aligned} \dot{\boldsymbol{\eta}} &= \mathbf{A}\boldsymbol{\eta} + \mathbf{B}\varepsilon \\ \dot{\boldsymbol{v}} &= \mathbf{S}\boldsymbol{v} + \boldsymbol{\Gamma}\mathbf{C}\boldsymbol{\eta} \\ y &= \boldsymbol{\Gamma}^T\boldsymbol{v}. \end{aligned} \tag{10}$$

The generalized Lyapunov demodulator (10) is a linear time-invariant (LTI) system, thus ensuring the applicability of common control design techniques, in contrast to the standard Lyapunov demodulator (2).

A block diagram of the generalized demodulator is shown in Fig. 1, where $K(s)$ represents the system (9), and $G(s)$ represents the transfer function of the system (8) with $\gamma = 1$, as $\gamma$ is replaced by $K(s)$. By virtue of the *internal model principle*, we have

$$G(s) = \frac{s}{s^2 + \omega_c^2}. \tag{11}$$

The corresponding closed-loop response $T(s)$ is given by

$$T(s) = \frac{G(s)K(s)}{1 + G(s)K(s)}. \tag{12}$$

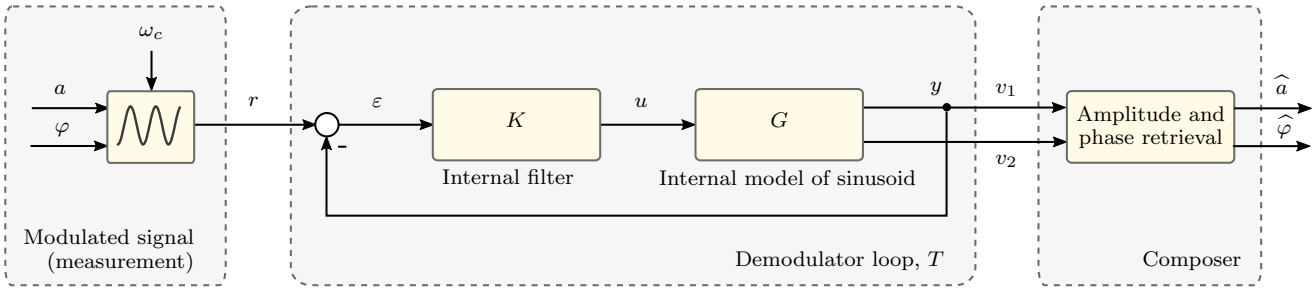


Fig. 1. Structure of the generalized Lyapunov demodulator by the internal model principle, ensuring perfect tracking in the stationary case. The internal filter $K(s)$ can be designed to match the requirements of the demodulator.

Then, we can use any standard technique in the frequency-domain to shape the open-loop $L(s) = G(s)K(s)$ or closed-loop $T(s)$, or we could work in the time-domain by selecting $\mathbf{A}, \mathbf{B}, \mathbf{C}$ in (9).

*Remark 1.* The sinusoidal input signal is treated as a reference signal to be tracked. By the internal model principle, perfect tracking in the stationary sense is achieved by the general Lyapunov demodulator for any stable filter $K(s)$.

### *3.3 Retrieval of Amplitude and Phase*

In order to use (8) or (10), a transformation from $\boldsymbol{v}$ to $\boldsymbol{x}$ appears to be necessary in order to obtain the estimated amplitude and phase from (4), i.e. by using

$$\boldsymbol{x} = \left(e^{\mathbf{S}t}\right)^{-1} \boldsymbol{v}. \tag{13}$$

Instead, note that $e^{\mathbf{S}t}$ is a rotation matrix in the group SO(2) with angle $-\omega_c t$ (Spong et al., 2005). Thus, magnitude is preserved through the transformation (13) while the angle decreases linearly with time. By this observation, the transformation is not necessary, and the estimated amplitude and phase can be recovered directly and efficiently by using

$$\hat{a} = \sqrt{v_1^2 + v_2^2}, \tag{14}$$

$$\hat{\varphi} = \left(\left(\operatorname{atan2}\left(v_1, v_2\right) - \omega_c t + \pi\right) \mod 2\pi\right) - \pi. \tag{15}$$

where the modulus operator and $\pi$-terms ensure $\hat{\varphi} \in [-\pi, \pi)$.

*Remark 2.* This observation leads to the interpretation that the states $\boldsymbol{x}$ of the Lyapunov demodulator (2) operates in a reference system rotating with the carrier frequency; thereby achieving constant states for constant amplitude and phase, as opposed to the sinusoidally rotating states of $\boldsymbol{v}$ in (8).

### *3.4 Tracking Bandwidth*

In order to guide the design of the demodulator filters for tracking time-varying amplitude and phase, the passband of the demodulator loop is examined. Consider an input signal with sinusoidally varying amplitude $a(t) = a_0 + m_0 \cos \omega_m t$ for some constants $\omega_m, a_0 > 0$ and $m_0 < a_0$. Then, we have

$$\begin{aligned} r(t) &= a(t) \sin \omega_c t \\ &= (a_0 + m_0 \cos \omega_m t) \sin \omega_c t \\ &= a_0 \sin \omega_c t + \tfrac{1}{2} m_0 \sin\left[(\omega_c - \omega_m)t\right] \\ &\quad + \tfrac{1}{2} m_0 \sin\left[(\omega_c + \omega_m)t\right]. \end{aligned} \tag{16}$$

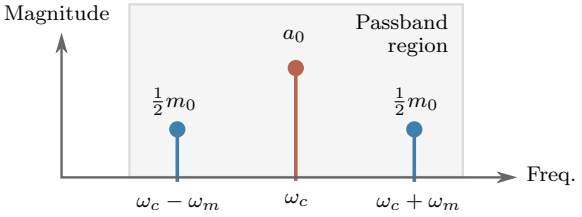


Fig. 2. The modulation products of a sinusoidal amplitude signal. In order to track a modulated signal of $\omega_m$ frequency, the demodulator loop must have a passband region covering $\omega_c \pm \omega_m$.

Thus, in the frequency domain, the modulation products are moving away from the carrier frequency with increasing $\omega_m$, as shown in Fig. 2. Therefore, the amplitude and phase tracking bandwidth $\omega_b$ is about half the passband bandwidth in $T(s)$, taking into consideration that the bandpass filter may not be exactly symmetric around $\omega_c$.

## 4. DIRECT CLOSED-LOOP FILTER DESIGN

The generalized demodulator structure (10) allows for the direct design of demodulators with distinct features such as a specific order and filter shape. One approach is to design $K(s)$ while keeping $G(s)$ fixed by using traditional control design techniques. However, only a limited class of controllers is admissible for a given overall desired closed-loop demodulator characteristic (Ruppert et al., 2018).

Instead, a more flexible approach is the direct design of the closed-loop filter $T(s)$. As long as the conditions

$$|T(j\omega_c)| = 1, \quad \angle T(j\omega_c) = 0\,^\circ, \tag{17}$$

are satisfied, then the perfect tracking condition still applies. The conditions (17) ensure that $T(j\omega_c) = 1$, resulting in a stationary tracking error of zero. Otherwise, the conditions can be relaxed in order to improve the filter response over the entire tracking bandwidth.

### *4.1 Recovering Amplitude and Phase*

In the direct closed-loop design approach, only the output of $T(s)$ is available which is insufficient for resolving the amplitude and phase estimates. However, this can be resolved by taking advantage of the internal model described by (10). Here, we have $\dot{v}_2 = -\omega_c v_1$. Thus, an equivalent transfer function for the second state is obtained by

$$T^{\perp}(s) = -\tfrac{\omega_c}{s} T(s). \tag{18}$$

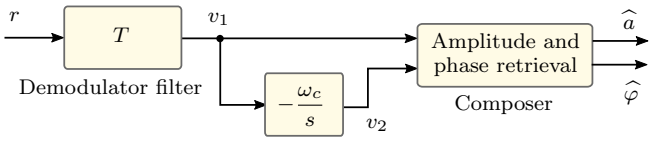


Fig. 3. Equivalent direct closed-loop design approach. Here, $T(s)$ is designed directly as a bandpass filter.

As in the internal model, this ensures a 90° phase difference between the two states. Thus, once the closed-loop filter $T(s)$ is designed, the second state is retrieved by (18). Then, the output of $T(s), T^{\perp}(s)$ can be used as $v_1, v_2$ respectively to retrieve the amplitude and phase by (14)–(15) as illustrated in Fig. 3.

### *4.2 Filter Design Considerations*

It is clear from the discussion in Sec. 3.4 that the filter $T(s)$ should be designed as a bandpass filter with center frequency near $\omega_c$ and a passband bandwidth about twice the tracking bandwidth desired. Several other considerations should be recognized during the design of the filter.

*Amplitude and Phase Offsets* If the designed filter $T(s)$ does not satisfy unity magnitude and zero-phase at $\omega_c$ as in (17), then the resulting amplitude and phase will be biased for the case of constant amplitude and phase. The corrected estimates $\hat{a}_c, \hat{\varphi}_c$ can be obtained from

$$\hat{a}_c = \frac{\hat{a}}{|T(j\omega_c)|}, \quad \hat{\varphi}_c = \hat{\varphi} - \angle T(j\omega_c). \tag{19}$$

*Relative Filter Order* The relative filter order is directly related to the magnitude rolloff outside the bandwidth of the signal. This is the prime determining factor for off-mode rejection. In applications such as multifrequency AFM, multiple demodulators can be added together such that each $T(s)$ do not overlap for the carrier frequencies considered. Thus, the steeper rolloff of higher relative order filters allows increased bandwidth without overlap.

*Phase Delay* The transient performance is partly determined by the phase delay. In general, a lower-order filter will have a smaller phase delay and improved transient performance, leading to a trade-off between filter order and performance. However, filters of the same order can achieve different steepness of the phase within the passband region, which should be considered during the design of the filter $T(s)$. A minimum-phase filter is desirable.

*Group Delay* The group delay – that is, the derivative of phase w.r.t. frequency – of a filter $T(s)$ should ideally be near-constant inside the passband region (Lyons, 2010). A non-constant group delay will make the emergence of sidebands such as in Fig. 2 appear with different time-delays, and can thus be detrimental to the tracking in the transient regime, as demonstrated later.

## 5. FILTER EXAMPLES

The generalized Lyapunov demodulator is highly flexible in terms of filter choice. In this section, several specific filters with different characteristics are suggested for use in the direct design approach of the generalized Lyapunov demodulator, applied as $T(s)$ in Fig. 3.

Table 1. Higher order Lyapunov demodulators.

| $i$ | $T_i(s)$ | $K_i(s)$ |
|---|---|---|
| 1 | $\frac{\gamma s}{s^2+\gamma s+\omega_c^2}$ | $\gamma$ |
| 2 | $\frac{\gamma^2 s^2}{(s^2+\gamma s+\omega_c^2)^2}$ | $\frac{\gamma^2 s}{s^2+2\gamma s+\omega_c^2}$ |
| 3 | $\frac{\gamma^3 s^3}{(s^2+\gamma s+\omega_c^2)^3}$ | $\frac{\gamma^3 s^2}{s^4+3\gamma s^3+(3\gamma^2+2\omega_c^2)s^2+3\gamma\omega_c^2 s+\omega_c^4}$ |
| 4 | $\frac{\gamma^4 s^4}{(s^2+\gamma s+\omega_c^2)^4}$ | $\frac{\gamma^4 s^3}{s^6+4\gamma s^5+(6\gamma^2+3\omega_c^2)s^4+(4\gamma^3+8\gamma\omega_c^2)s^3+(6\gamma^2\omega_c^2+3\omega_c^4)s^2+4\gamma\omega_c^4 s+\omega_c^6}$ |

### *5.1 Higher Order Lyapunov Filters*

The first approach considers a control design based on the standard Lyapunov demodulator. In order to achieve a better response in terms of off-mode rejection, higher order versions of the Lyapunov demodulator are designed. The closed-loop response $T(s)$ from (12) can be found for the standard Lyapunov demodulator where $K = \gamma$, which gives the transfer function (Ruppert et al., 2018)

$$T_1(s) = \frac{\gamma s}{s^2 + \gamma s + \omega_c^2}. \tag{20}$$

The higher order Lyapunov demodulators are then formulated as

$$T_i(s) = T_1(s)^i \tag{21}$$

where $i$ represents the relative order of the filter. The Lyapunov filters $T_i$ can either be implemented using the direct filtering approach as in Fig. 3, or can be implemented using the full control loop as in Fig. 1 by solving $T_i$ for $K_i$ with $G$ from (11), corresponding to the approach in Ruppert et al. (2018). The Lyapunov filters, either implemented using $T_i$ or $K_i$ are listed for relative orders 1–4 in Table 1.

### *5.2 Other Bandpass Filters*

In addition to the higher order Lyapunov filters, the following standard LTI filters are considered for use in the generalized Lyapunov demodulator. The filters are converted from lowpass form to bandpass form using standard transformation techniques (Antoniou, 2005). For the lowpass filters of order $n$, the resulting bandpass filters are order $2n$ and relative order $n$.

*Butterworth Filter* The magnitude of the Butterworth filter is maximally flat inside its passband region, however, there is no consideration for the resulting phase response.

*Bessel Filter* The Bessel filter has the characteristic of providing a maximally flat group delay, but generally has a less steep magnitude dropoff compared to the Butterworth filter.

*Chebyshev Filter* The Chebyshev type-I filter provides a very steep magnitude dropoff near the crossover frequency, at the expense of ripples in the passband region, a steep phase delay, and a highly variable group delay.

## 6. SIMULATION RESULTS

The filters described in the previous section are implemented using the direct design approach for demodulation of amplitude and phase. Numerical results are obtained in order to demonstrate the feasibility and flexibility of the generalized Lyapunov demodulator.

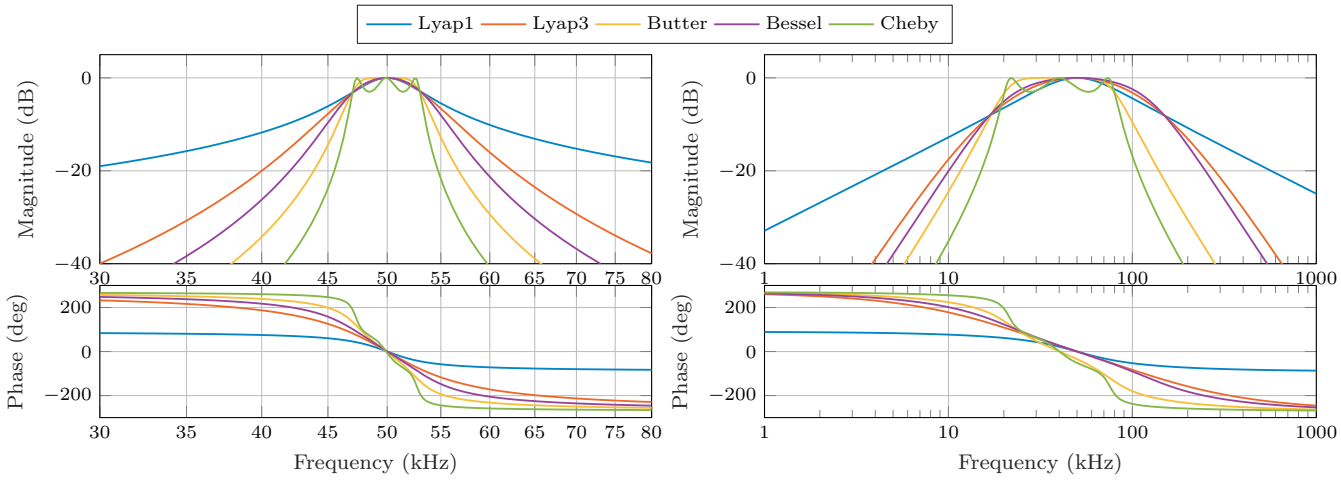


(a) 3 kHz bandwidth (b) 30 kHz bandwidth

Fig. 4. Bode plot of $T(s)$ for the implemented bandpass filters at **(a)** low and **(b)** high bandwidth settings.

### 6.1 Implementation Details

In addition to the standard Lyapunov demodulator (Lyap1), relative order 3 versions of the Lyapunov (Lyap3), Butterworth (Butter), Bessel, and Chebyshev (Cheby) filters are implemented for numerical evaluation. This enables a well founded comparison between the previous relative order 1 technique (Lyap1) and higher order filters, in addition to the comparison among several filters of the same order. The carrier frequency considered is 50 kHz, and the filters are implemented at a high and a low bandwidth setting, 30 kHz and 3 kHz respectively. Butter and Cheby are implemented for exact symmetry around $\omega_c$ at the expense of some deviation to the perfect tracking conditions (17) particularly visible for the high-bandwidth setting, while the others satisfy the conditions exactly. The Bode plots of the resulting filters, $T(s)$, are shown in Fig. 4 for both bandwidth settings.

### 6.2 Frequency Domain Tracking

The amplitude tracking frequency response is gathered by applying a sinusoidal reference amplitude $a(t) = a_0 + m_0 \sin(\omega_m t)$ for a constant $\omega_m$ at a time, and finding the magnitude of the estimated amplitude response at $\omega_m$ using a second-order Goertzel algorithm (Proakis and Manolakis, 1996). This procedure is then repeated for increasing $\omega_m$.

The resulting tracking magnitude over $\omega_m$ is plotted in Fig. 5. It is seen that Lyap1 is the worst at rejecting high-frequency components due to its $-20$ dB/dec rolloff. The other filters have a $-60$ dB/dec rolloff as they are relative order 3 filters. Cheby has the steepest dropoff at the expense of a non-flat magnitude inside the passband.

Magnitude distortions can be seen between $\omega_c$ and $2\omega_c$, especially for the high bandwidth setting. This is a result of the mixing products given in (16) being reflected off from the negative frequency domain and into the passband of the filters. Signal filtering techniques such as the multinotch could possibly attenuate the distortions (Abramovitch, 2015).

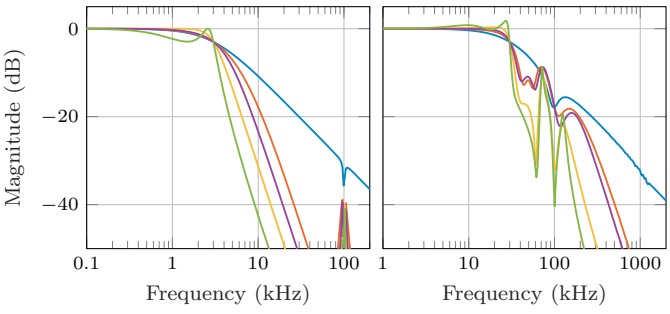


(a) 3 kHz bandwidth (b) 30 kHz bandwidth

Fig. 5. Amplitude tracking frequency response at **(a)** low and **(b)** high bandwidth settings. Colored as in Fig. 4.

### 6.3 Transient Tracking Performance

The transient performance is investigated by the tracking response to a step in the amplitude, shown in Fig. 6 for both bandwidth settings. It is seen that Lyap1 has the sharpest response time, while in particular Cheby is considerably slower. This can possibly be attributed to the steep phase of the Cheby filter inside the passband. Additionally, its highly variable group delay is considered to be the origin of the transient oscillations and large peaks visible. Lyap3 and Bessel are quite fast, with Butter trailing slightly behind.

### 6.4 Off-mode Rejection

The off-mode rejection for the various filters is indicated by the magnitude in $T(s)$ in Fig. 4. It is seen that Lyap1 has a considerable lower magnitude rolloff compared to the higher-order filters. This makes it less suitable for applications where multifrequency demodulation is required. A steep dropoff criteria favors Cheby in particular, but in general all the relative order 3 filters compare favorably to Lyap1.

In order to evaluate their differences numerically, an amplitude reference signal with frequency components outside the bandwidth of the demodulator is tracked. The amplitude signal is given by

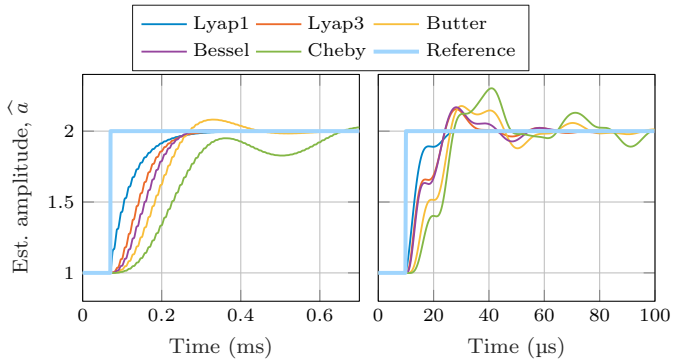


(a) 3 kHz bandwidth (b) 30 kHz bandwidth

Fig. 6. Amplitude step response of demodulators.

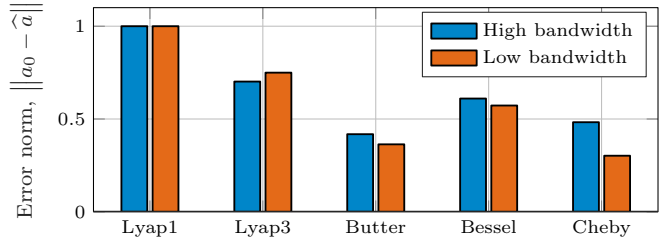


Fig. 7. Attenuation of harmonic frequency components outside the tracking bandwidth, favoring the higher order demodulators. The amplitude errors are normalized for comparison.

$$a(t) = a_0 + \sum_{k=1}^{10} a_k \sin(k \cdot \omega_m t + \varphi_k) \tag{22}$$

where we choose $\omega_m$ as twice the actual tracking bandwidth, $a_k = a_0/k$, and the constants $\varphi_k$ are chosen from a uniform random distribution. Ideally, only $a_0$ is tracked, while the harmonics of $\omega_m$ are completely attenuated.

The resulting error norms of the estimated amplitude $\hat{a}$ for both the high and low bandwidth demodulators are shown in Fig. 7. The results highly favor the higher order demodulators over Lyap1, in particular the Cheby and Butter filters. Bessel delivers a good compromise when both transient performance and off-mode rejection is considered.

## 7. CONCLUSIONS

In this article, the standard Lyapunov demodulator is equivalently recast as a reference tracking problem, with perfect tracking achieved by the internal model principle. It is shown that the generalized Lyapunov demodulator can be equivalently implemented by standard bandpass filters, while achieving perfect tracking under very light conditions. The approach results in a highly attractive combination of higher order filtering with high tracking bandwidth, simple implementation, and high flexibility for satisfying specific application requirements. Considerations for the design of the bandpass filter are discussed, and several standard filters have been explored in addition to higher order versions of the standard Lyapunov demodulator. Numerical examples compare the standard Lyapunov demodulator to relative order 3 versions of the Lyapunov demodulator, Butterworth, Bessel, and Chebyshev bandpass filters, all implemented for the generalized Lyapunov demodulator. The higher order filters achieve a greater rejection of off-mode components while retaining a high tracking bandwidth, thereby making the approach desirable for a wide array of applications, including multi-frequency AFM.

## REFERENCES

Abramovitch, D.Y. (2015). The multinotch, part I: A low latency, high numerical fidelity filter for mechatronic control systems. In *American Control Conference*. Chicago, USA.

Abramovitch, D.Y., Andersson, S.B., Pao, L.Y., and Schitter, G. (2007). A Tutorial on the Mechanisms, Dynamics, and Control of Atomic Force Microscopes. In *American Control Conference*. New York, USA.

Antoniou, A. (2005). *Digital Signal Processing: Signals, Systems and Filters*. McGraw-Hill, New York, 1 edition.

Cartagena-Rivera, A.X., Wang, W.H., Geahlen, R.L., and Raman, A. (2015). Fast, multi-frequency, and quantitative nanomechanical mapping of live cells using the atomic force microscope. *Scientific Reports*, 5, 11692.

Dufrêne, Y.F., Ando, T., Garcia, R., Alsteens, D., Martinez-Martin, D., Engel, A., Gerber, C., and Müller, D.J. (2017). Imaging modes of atomic force microscopy for application in molecular and cell biology. *Nature Nanotechnology*, 12(4), 295–307.

Francis, B.A. and Wonham, W.M. (1976). The internal model principle of control theory. *Automatica*, 12(5), 457–465.

Garcia, R. and Perez, R. (2002). Dynamic atomic force microscopy methods. *Surface science reports*, 47(6-8), 197–301.

Garcia, R. and Herruzo, E.T. (2012). The emergence of multifrequency force microscopy. *Nature Nanotechnology*, 7(4), 217–226.

Goodwin, G.C., Graebe, S.F., and Salgado, M.E. (2000). *Control System Design*. Prentice Hall.

Harcombe, D.M., Ruppert, M.G., Ragazzon, M.R.P., and Fleming, A.J. (2018). Lyapunov estimation for high-speed demodulation in multifrequency atomic force microscopy. *Beilstein Journal of Nanotechnology*, 9(1), 490–498.

Herruzo, E.T., Perrino, A.P., and Garcia, R. (2014). Fast nanomechanical spectroscopy of soft matter. *Nature communications*, 5, 3126.

Lyons, R.G. (2010). *Understanding Digital Signal Processing*. Prentice Hall, Upper Saddle River, NJ, 3rd edition.

Messineo, S. and Serrani, A. (2009). Offshore crane control based on adaptive external models. *Automatica*, 45(11), 2546–2556.

Proakis, J.G. and Manolakis, D.G. (1996). *Digital Signal Processing: Principles, Algorithms, and Applications*. Prentice Hall, Upper Saddle River, NJ, 3rd edition.

Ragazzon, M.R.P., Gravdahl, J.T., and Pettersen, K.Y. (2018a). Model-Based Identification of Nanomechanical Properties in Atomic Force Microscopy: Theory and Experiments. *IEEE Transactions on Control Systems Technology*.

Ragazzon, M.R.P., Ruppert, M.G., Harcombe, D.M., Fleming, A.J., and Gravdahl, J.T. (2018b). Lyapunov Estimator for High-Speed Demodulation in Dynamic Mode Atomic Force Microscopy. *IEEE Transactions on Control Systems Technology*, 26(2), 765–772.

Ruppert, M.G., Harcombe, D.M., and Moheimani, S.O.R. (2016). High-Bandwidth Demodulation in MF-AFM: A Kalman Filtering Approach. *IEEE/ASME Transactions on Mechatronics*, 21(6), 2705–2715.

Ruppert, M.G., Harcombe, D.M., Moore, S.I., and Fleming, A.J. (2018). Direct Design of Closed-loop Demodulators for Amplitude Modulation Atomic Force Microscopy. In *American Control Conference*. Milwaukee, WI, USA.

Ruppert, M.G., Harcombe, D.M., Ragazzon, M.R.P., Moheimani, S.O.R., and Fleming, A.J. (2017). A review of demodulation techniques for amplitude-modulation atomic force microscopy. *Beilstein Journal of Nanotechnology*, 8(1), 1407–1426.

Spong, M.W., Hutchinson, S., and Vidyasagar, M. (2005). *Robot Modeling and Control*. Wiley.